Journal of Biomedical Optics 7(2), 236–243 (April 2002)

Influence of optical properties and fiber separation on laser doppler flowmetry

Marcus Larsson
Linköpings Universitet
Department of Biomedical Engineering
Linköping, Sweden

Wiendelt Steenbergen
University of Twente
Faculty of Applied Physics
Enschede, The Netherlands

Tomas Strömberg
Linköpings Universitet
Department of Biomedical Engineering
Linköping, Sweden

Abstract. Microcirculatory blood flow can be measured using a laser Doppler flowmetry (LDF) probe. However, the readings are affected by the tissue's optical properties (absorption and scattering coefficients, μ_a and μ_s) and probe geometry. In this study the influence of optical properties [$\mu_a \in (0.053,0.23)$ mm^{-1}, $\mu_s \in (14.7,45.7)$ mm^{-1}] on LDF perfusion and LDF sampling depth was evaluated for different fiber separations. *In vitro* measurements were made on a sophisticated tissue phantom with known optical properties that mimicked blood flow at different depths. Monte Carlo simulations were carried out to extend the geometry of the tissue phantom. A good correlation between measured and simulated data was found. The simulations showed that, for fixed flow at a discrete depth, the influence of μ_s or μ_a on LDF perfusion increased with an increase in flow depth and decreased with an increase in fiber separation. For a homogeneous flow distribution, however, the perfusion varied 40% due to variations in the optical properties, almost independent of the fiber separation (0.23–1.61 mm). Therefore, the effect in real tissue is likely to vary due to the unknown heterogeneous blood flow distribution. Further, the LDF sampling depth increased with a decrease in μ_s or μ_a and an increase in fiber separation. For fiber separation of 0.46 mm, the e^{-1} sampling depth ranged from 0.21 to 0.39 mm. [DOI: 10.1117/1.1463049]

Keywords: Doppler effect; fiber optics; laser Doppler flowmetry; Monte Carlo simulations; optical properties; sampling depth.

Paper JBO-001013 received Feb. 22, 2001; revised manuscript received Aug. 24, 2001; accepted for publication Dec. 11, 2001.

1 Introduction

Skin perfusion measurements using the laser Doppler technique depend on how the light interacts with moving blood cells and static tissue. The measurement situation is complex due to the heterogeneous vascular structure. This structure includes both superficial capillaries with a relatively low velocity of blood cells and larger vessels, deeper in the skin, with higher velocities of blood. Therefore, the probability for light interaction with moving blood cells is not only affected by the distribution of blood cells in tissue but also by the penetration depth of detected photons, i.e., the sampling depth.[1] Recently Liebert et al. have experimentally shown, using a layered flow model and a multichannel laser Doppler flowmetry (LDF) probe, that the sampling depth increases with an increase in separation between emitting and receiving fibers.[2] They suggested that such a system could be used to discriminate between superficial and deeper lying blood vessels. Similar results regarding the influence of probe geometry on the LDF sampling depth were obtained by Johansson et al. during studies of isolated segments of feline small intestine.[3] The sampling depth has also been studied theoretically using either a Monte Carlo simulation model[4,5] or a lattice random-walk model.[6] The latter two reports did not only show that the sampling depth increases with fiber separation but also that it is affected by the optical properties of the tissue. In addition, Weiss et al.[6] showed that the sampling depth decreases with the absorption coefficient. However, their results were restricted to fiber separations larger than 1 mm, a range in which LDF is rarely used. It has been observed that LDF perfusion varies both intra- and interindividually.[7] The origin of these variations is rather complex and might, as described above, not only depend on the concentration of moving blood cells, blood velocity, and vascular structure, but also on the tissue's optical properties. To our knowledge, no systematic study of the influence of tissue optical properties, flow depth and probe geometry on LDF perfusion has previously been presented.

In the present study, we show how LDF perfusion is affected by flow depth, fiber separation and optical properties relevant to skin. A sophisticated tissue phantom, with known geometry and optical properties, and a Monte Carlo model that mimicks the tissue phantom have been used. Both the tissue phantom and the simulation model consisted of a number of static layers with different optical properties, separated by moving layers. Thereby a range of different discrete flow depths and optical properties was possible to evaluate. Good agreement between measurements and simulations was found within the geometrical accuracy of the tissue phantom. Since

Address all correspondence to Marcus Larsson. Tel: +46-13-222487; Fax: +46-13-101902; E-mail: marla@imt.liu.se. A preliminary report was published in Proc. SPIE **3923**, 56–63 (2000).

1083-3668/2002/$15.00

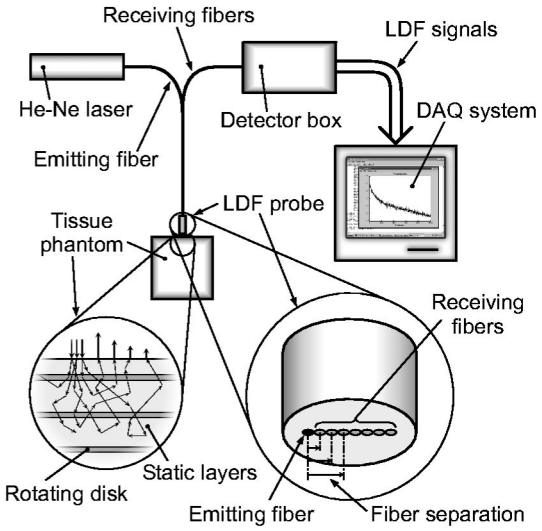

Fig. 1 LDF system, including a tissue phantom that simulates flow, and a custom made LDF probe with different emitting–receiving fiber separations. The light intensity detected in each receiving fiber was sampled by a data acquisition system (DAQ) in terms of the time varying signal (ac) and the light intensity signal (dc).

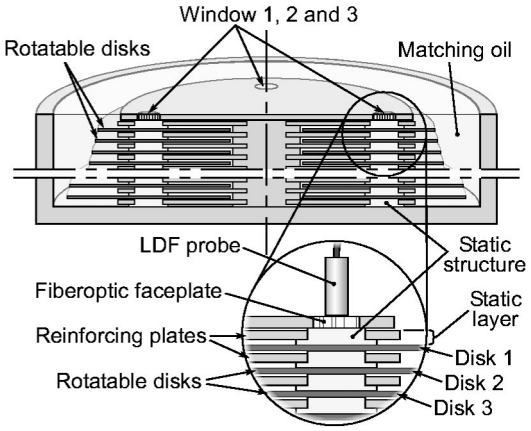

Fig. 2 Cross section of the tissue phantom, illustrating two of the four stacks of static structure separated by a number of rotatable disks. All layers are separated by index matching oil. The magnification shows the arrangement of the LDF probe, the fiberoptic face plate (window), rotatable structures and static layers.

the geometry of a simulation model is easier to control than a physical phantom, the main conclusions of the study were based on a refined and extended simulation model. We also show how changes in the optical properties of a homogeneous flow distribution model affect the LDF perfusion using Monte Carlo simulations. Further, in this paper we quantify and describe how the optical properties and the fiber separation affect the e^{-1} LDF sampling depth.

2 Methods and Apparatus

2.1 Data Acquisition

A digital multichannel LDF probe system (Figure 1) was used to estimate the perfusion generated by a tissue phantom. The LDF system consisted of a 632.8 nm He–Ne laser connected to the LDF probe via one emitting fiber. Backscattered light was guided to a detector system via seven receiving fibers arranged in a row. Multimode step index fibers [numerical aperture (NA) = 0.37] with a diameter of 230 μm (including 30 μm of cladding) were used. The distances between the center of the emitting fiber and the center of the receiving fiber (fiber separation) was $230n$ μm, n = 1,2,3, . . . ,7.

Backscattered light from each of the seven receiving fibers was detected by two photodetectors. By adding the two photocurrents the light intensity (dc signal) of the LDF signal was detected. The time varying part (ac signal) of the LDF signal was identified by subtracting the photocurrents, amplifying and band pass filtering with a third order Butterworth filter between 20 Hz and 12.5 kHz. By using a differential detector approach, common mode noise was reduced.[8] Due to the low signal to noise ratio (SNR) of the ac signals of fibers 6 and 7, these fibers were not used for measurements in this study.

The filtered ac and dc signals were sampled at 50 kHz with a 12-bit data acquisition card (MIO-AT-16-10E, National Instruments Corporation) using a range of ±10 V. All data acquisition software was developed using LabView 5.0 (National Instruments Corporation).

2.2 Tissue Phantom

The tissue phantom (Figure 2) consisted of a number of parallel rotatable disks, with thicknesses of 20–22 μm. Each of these disks was separated from each other by a static layer (approximately 95 μm thick) that contained four pieces of static structure with different optical properties. These pieces were located at the same radial distance from the center of the tissue phantom, with an offset of 90°. All together, the static layers were arranged in a way that resulted in four different stacks of static structures, each with the same optical properties. This assembly was placed in a container filled with index matching fluid (Leica index matching oil). The container was covered by a plate that had four fiber-optic face plates (windows) through which the laser Doppler probes had optical access to the tissue phantoms. These windows (w_1–w_4) provided a mechanical barrier, but did not affect the spatial distribution of either the incoming laser beam or light escaping from the phantom tissue. All static layers belonging to the same window had the same optical properties. The rotating disks and the static layers were made of a mixture of polyvinyl alcohol and hollow polystyrene microspheres. These microspheres, with diameters of 1 μm, served as photon scatterers. In addition, various nonscattering dyes (optical absorbers) were added to the static layers. The anisotropy ($\langle \cos\theta \rangle$, θ = scattering angle) of the disks and the layers was 0.8–0.83. The scattering coefficient μ_s and absorption coefficient μ_a of the tissue phantom, for a wavelength of 633 nm, are given in Table 1. The scattering coefficient and the absorption coefficient were determined by transmission measurements in a Shimadzu UV-2101PC photospectrometer. The scattering coefficient was determined by measuring the collimated transmission through different numbers of reference samples without dyes, hence with zero absorption. An exponential decrease in the collimated light transmission with the total sample thickness was found. Hence, μ_s could be determined by an exponential fit. A similar procedure, with refer-

Table 1 Optical properties of the static windows and the rotating disks for the tissue phantom and the simulation models.

	Window 1	Window 2	Window 3	Window 4	Rotating disks
Scattering coefficient μ_s (mm^{-1})	14.66	44.85	14.80	45.55	7.4 ± 0.1
Absorption coefficient μ_a (mm^{-1})	0.212	0.226	0.0405	0.0532	~0

ence samples that only contained dyes, i.e., with zero scattering, was carried out to determine μ_a. The anisotropy was determined for a wavelength of 636 nm by measuring the angular dependence of the transmission, i.e., the phase function, through thin samples with zero absorption. A sufficiently low scattering level was used to ensure single scattering. This method for measuring the scattering phase function was described earlier by Bolt et al.[9] All reference samples were from the same batches of raw materials (polyvinyl alcohol solution, particles and dyes) as the layers and disks of the tissue phantom. Also, the same index matching fluid as that in the tester was used. A more thorough description of the optical tissue phantom used in this study was presented by Steenbergen and de Mul.[10–12]

Measurements were made using single moving disks at 4 different depths and 11 different velocities, equally distributed in the range of 0–3.6 mm/s. The disk depth was not the same for window 4 as it was, for window 1 and window 2, where one extra static layer was present between disk 2 and disk 3. All disk depths (the distance between the phantom's surface and the center of the rotating disk) that were used are shown in Table 2. Due to problems with air bubbles in window 3, LDF measurements were made only on window 1 (w_1), window 2 (w_2), and window 4 (w_4).

2.3 Signal Processing

According to laser Doppler theory, measured perfusion, Perf_M, can be estimated as[1,13]

$$\mathrm{Perf}_M = \frac{\sum_{\omega_d} \omega_d \cdot P_M(\omega_d)}{\mathrm{dc}_M^2}, \tag{1}$$

where $P_M(\omega_d)$ is the measured Doppler power spectrum, ω_d is the angular frequency of the Doppler shift ($\omega_d : 0 \mapsto 12\,500$ Hz), and dc_M is the measured total light intensity.

The Doppler spectrum was calculated as a mean over 50 power spectra, where each power spectrum was estimated from 4096 samples of the corresponding ac signal. The dc values were calculated as a mean over 10 000 samples. Calibration of all dc values was carried out by normalizing each channel with its relative amplification factor derived by emitting a constant amount of light into each fiber. This procedure made it possible to compare simulated and measured dc decay as a function of the fiber separation.

Since the tissue phantom uses a rotating rigid lattice of scattering and absorbing particles to simulate flow, the number of moving scatters is constant. Therefore, as long as the maximal Doppler frequency of the backscattered light is lower than the cut off frequency of the low pass filter (12 500 Hz), perfusion will vary linearly with the disk velocity v_{disk}:[14]

$$\mathrm{Perf}_M(v_{\mathrm{disk}}) = k v_{\mathrm{disk}} + U_{\mathrm{bias}}. \tag{2}$$

The slope k, quantified with linear regression, was used as the measured perfusion value for a disk velocity of 1 mm/s. The perfusion bias U_{bias} compensates for signal noise. All calculations were made using Matlab 5.2 (The MathWorks, Inc.).

Table 2 Average disk depth of rotating disks (and thickness) in μm for the tissue phantom.

	Disk 2	Disk 4	Disk 6	Disk 8
Window 1 and window 2 (μm)	190 (21)	421 (22)	653 (22)	885 (22)
Window 4	190 (21)	516 (22)	748 (22)	980 (22)

2.4 Simulation Model

To further understand how photons migrate through a turbid medium, such as in the tissue phantom used in this study, a mathematical model is needed. Due to the need for registering the photon Doppler shifts, the complexity of the measurement setup and the tissue phantom structure, a Monte Carlo simulation approach was chosen. With this technique, it is possible to simulate the pathway of individual photons if the scattering coefficient, absorption coefficient, and phase function of the medium are known. A short review and comparison of the Monte Carlo technique with measurements and diffusion theory was presented earlier by Flock et al.[15,16]

For the Monte Carlo simulations, the same geometrical configuration and optical characteristics as those for the tissue phantom were modeled using a disk velocity of 1 mm/s (model 1). The probability distribution of the photon scattering angle was modeled using the Henyey–Greenstein phase function ($g = 0.815$).[17] To compare LDF spectra, Monte Carlo simulations using one set of optical properties (window 1) and one single rotating disk (disk 2) were carried out for two of the velocities (0.7 and 2.2 mm/s) that were used in the LDF measurements. Furthermore, an extended simulation model (model 2) with the same geometric configuration for all windows and the same optical properties as the tissue phantom was designed. This model was evaluated for both single moving disks and multiple moving disks (all disks), using a disk velocity of 1 mm/s. Simulated disk depths using model 2 are shown in Table 3. Each simulation was carried out for a fixed number of detected photons (500 000), using software developed by de Mul et al.[18]

Table 3 Average disk depth (in μm) of rotating disks for the extended simulation model (model 2). The thickness of all rotating disks was 21 μm.

Disk No.	1	2	3	4	5	6	7	8	9	10	11
Disk depth (μm)	71	187	303	419	535	651	767	883	999	1115	1231

Since a ring shaped detector was used in the simulations, all photons had to be weighted differently depending on their detection radius (see the Appendix). The photon weight factor or intensity p_i is given by

$$p_i = \frac{1}{\pi}\cos^{-1}\left(\frac{r_i^2 + L(r_i)^2 - R_{\text{fiber}}^2}{2r_i \cdot L(r_i)}\right), \tag{3}$$

where p_i is the intensity of photon i, r_i is the detection radius of photon i, $L(r_i)$ is the emitting–receiving fiber separation (depending on r_i), and R_{fiber} is the radius of the receiving fiber core (100 μm).

Simulated light intensity, $\text{dc}_{S,n}$, was estimated by summing all the photon intensities detected by fiber n:

$$\text{dc}_{S,n} = \sum_{i_n}^{N_n} p_{i_n}, \tag{4}$$

where i_n are all photons detected by fiber n, p_{i_n} is the intensity of photon i_n, and N_n is the number of photons detected by fiber n.

The simulated Doppler power spectrum was estimated by first calculating the frequency distribution $H_{S,n}(k)$ of the simulated photons, detected by fiber n. A fixed frequency resolution Δf of 12 500/512$\approx$24.4 Hz and a frequency interval of (−12 500, 12 500) Hz were used. Hence, $H_{\text{sim},n}(k)$ is given by

$$H_{S,n}(k) = \sum_{i_n}^{N_n} p'_{i_n} \times \begin{bmatrix} p'_{i_n} = p_{i_n}, & \text{when } f_{d,i_n} \in [(k-1/2)\Delta f, (k+1/2)\Delta f], \\ p'_{i_n} = 0, & \text{when } f_{d,i_n} \notin [(k-1/2)\Delta f, (k+1/2)\Delta f], \\ k: -512 \mapsto 512; & \Delta f = 12\,500/512 \text{ Hz}. \end{bmatrix} \tag{5}$$

f_{d,i_n} is the Doppler shift of photon i_n (detected by fiber n).

The power spectrum $P_{S,n}(k)$ was obtained by convoluting the frequency distribution $H_{S,n}$ with itself.[18] The corresponding perfusion value was estimated as

$$\text{Perf}_{S,n} = \frac{\sum_k 2\pi k \Delta f P_{S,n}(k)}{\text{dc}_{S,n}^2}. \tag{6}$$

2.5 Influence of Optical Properties

The effect of differences in optical properties on LDF perfusion was evaluated by comparing the two perfusion values $\text{Perf}(OP_a, d, l)$ and $\text{Perf}(OP_b, d, l)$. Both these values were simulated using the same disk depth (d) and fiber separation (l), but two different sets of optical properties (OP_a and OP_b). The ratio, denoted $\Delta\text{Perf}(OP_a, OP_b, d, l)$, between these two perfusion values was defined as

$$\Delta\text{Perf}(OP_a, OP_b, d, l) = \frac{\text{Perf}(OP_a, d, l)}{\text{Perf}(OP_b, d, l)}. \tag{7}$$

This ratio indicates how perfusion is altered when the optical properties change from OP_a to OP_b. By selecting OP_a and OP_b wisely, the influence of either absorption or the scattering coefficient can be evaluated.

The maximal influence of optical properties on LDF perfusion, i.e., *the maximum perfusion variation*, was evaluated for each fiber separation between 0.23 and 1.61 mm by calculating the ratio

$$\frac{\max_{OP}[\text{Perf}(OP, d, l)]}{\min_{OP}[\text{Perf}(OP, d, 1)]}. \tag{8}$$

Both the homogeneous flow distribution model (simulation model 2 with all disks moving) and the discrete flow depth model (simulation model 2 with single disks moving) were evaluated by calculating the maximum perfusion variation.

2.6 Sampling Depth

The LDF sampling depth, as a function of the optical properties and fiber separation, was defined as the disk depth at which the perfusion had decayed to e^{-1} of the maximal perfusion. Due to a limited number of perfusion values, linear interpolation was used to estimate the sampling depths.

3 Results

3.1 dc Decay: Measured and Simulated

A good correlation between measured and simulated (model 1) dc decay was found (Figure 3). This indicates that the optical properties and the Monte Carlo model were correct. Both the measured and simulated dc values were normalized against the dc value of fiber 3 and window 2, thereby eliminating differences in amplification between the measurements and the simulations.

3.2 Doppler Power Spectra: Measured and Simulated

For the two velocities simulated, a good agreement between the frequency distribution of measured and simulated Doppler power spectra was found (Figure 4). This indicates that the Henyey–Greenstein phase function and the anisotropy ($g = 0.815$) of the simulation models are appropriate.

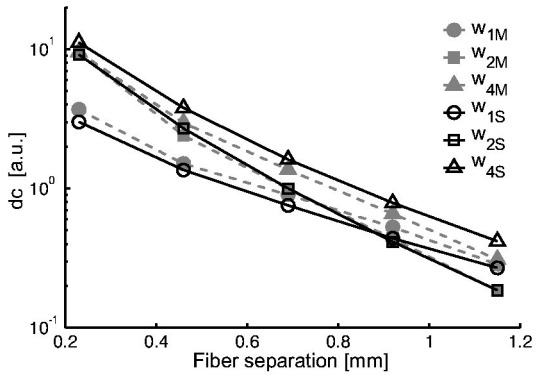

Fig. 3 Simulated (model 1; solid lines and open symbols) and measured (dashed lines and closed symbols) dc decay as a function of the fiber separation for the optical properties of windows 1, 2, and 4 (*S* =simulated; *M*=measured).

3.3 Perfusion Decay: Measured and Simulated

Simulated and measured perfusion as a function of the disk depth is presented in Figure 5 for fiber 1 and fiber 4. To eliminate differences in amplification all values were normalized against the maximum perfusion detected by each fiber. The result shows that the perfusion decay is faster for fiber 1 than for fiber 4. There is also an increase in perfusion decay with an increase in μ_s ($OP_{w_1} \rightarrow OP_{w_2}$) or an increase in μ_a ($OP_{w_4} \rightarrow OP_{w_2}$). In comparing simulated perfusion decay with measured perfusion decay a small but systematic discrepancy that increases with the disk depth is seen.

3.4 Influence of Optical Properties on Simulated LDF Perfusion

Model 2 was used to evaluate the influence of optical properties on LDF perfusion. The result, presented in Figure 6, indicates that the influence of either μ_s or μ_a on LDF perfusion increased with an increase in flow depth and decreased with an increase in fiber separation. Figure 6 also shows that the influence of μ_s on LDF perfusion increased with the magnitude of μ_a [Figure 6(a) vs 6(b)] and the influence of μ_a on LDF perfusion increased with the magnitude of μ_s [Figure 6(c) vs 6(d)].

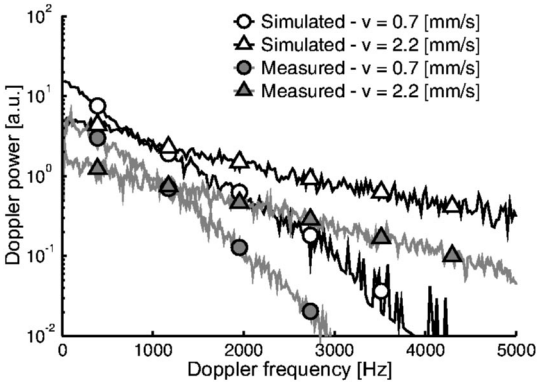

Fig. 4 Simulated (model 1; open symbols) and measured (closed symbols) Doppler power spectra for two different rotating disk velocities (0.7 and 2.2 mm/s), using window 1, disk 2, and fiber 1.

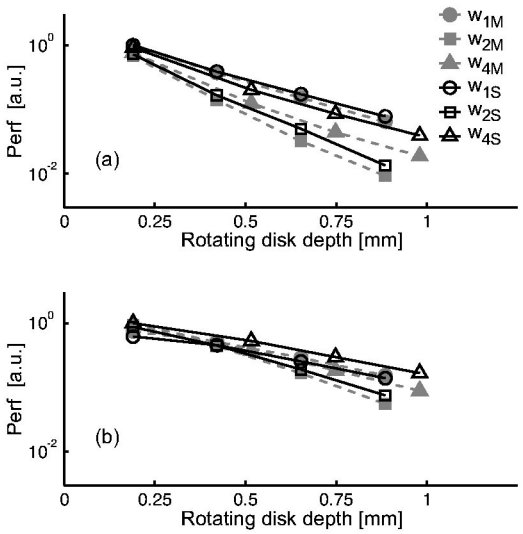

Fig. 5 Simulated (model 1; solid lines and open symbols) and measured (dashed lines and closed symbols) perfusion as a function of the disk depth for fiber 1 (a) and fiber 4 (b) (*S*=simulated;*M* =measured).

The maximum perfusion variation in the simulation data (model 2 using both single and multiple moving disks), as a function of fiber separation, is presented in Figure 7. For the homogeneously distributed flow model (all disks moving) the maximum variation in perfusion was on average 40%, ranging from 22% to 50%, for fiber separations between 0.23 and 1.61 mm. In general, all single moving disk models resulted in larger variations than in the model with all disks moving. There was also an increase in the maximum perfusion variation with an increase in disk depth. However, a decrease in variation with an increase in fiber separation could be noticed for disk 3 and below (>0.3 mm).

3.5 Sampling Depth: Simulated

The LDF sampling depth was evaluated using simulation model 2. The result, shown in Figure 8, indicates that the LDF sampling depth increases with a decrease in μ_s (w_2 vs w_1 and w_4 vs w_3) or μ_a (w_1 vs w_3 and w_2 vs w_4). The sampling depth also tends to increase linearly with fiber separation. According to the simulations the sampling depth for fiber 2 (0.46 mm fiber separation) is 0.21–0.39 mm.

4 Discussion

4.1 Validity of the Simulations

There was good agreement between measured and simulated dc decay (Figure 3) and LDF power spectrum (Figure 4). This strengthens the validity of the optical properties and the Monte Carlo simulation model. However, perfusion as a function of the flow depth (Figure 5) showed a small systematic mismatch between measured and simulated values. The difference tended to increase almost linearly with the flow depth. The most likely explanation for this is that the disk depths of the tissue phantom presented are slightly smaller than the actual disk depths due to the matching oil between the rotating disks and the static windows. The agreement between mea-

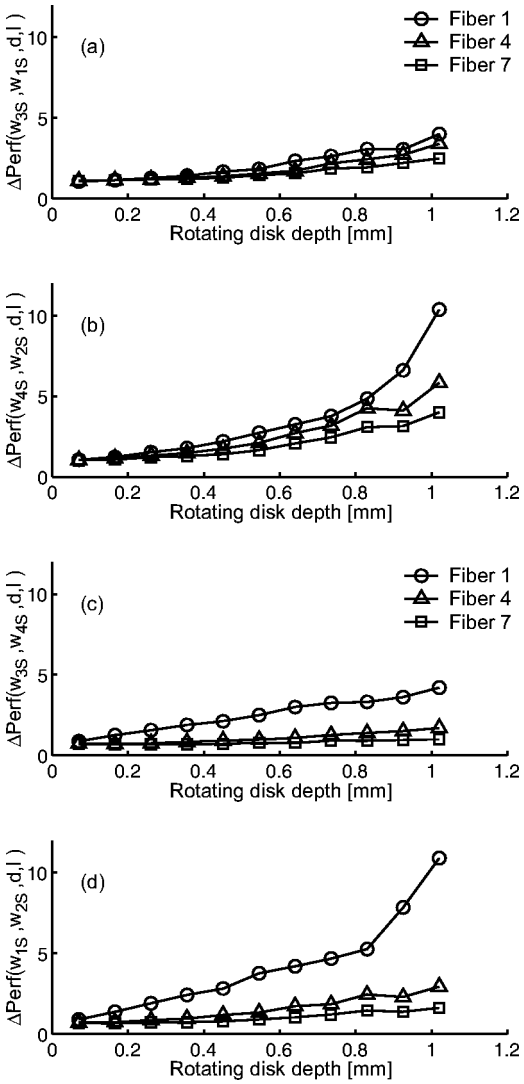

Fig. 6 Influence of the optical properties on the simulated LDF perfusion (model 2) for a range of rotating disk depths. The relative change in perfusion (ΔPerf) due to variations in μ_a (a), (b) or in μ_s (c), (d) is presented for fibers 1, 4, and 7. (a) μ_a: 0.0405→0.212 mm^{-1}, μ_s ≈15 mm^{-1}; (b) μ_a: 0.0532→0.226 mm^{-1}, μ_s≈45 mm^{-1}; (c) μ_s: 14.80→45.55 mm^{-1}; μ_a≈0.05 mm^{-1}; (d) μ_s: 14.66 →44.85 mm^{-1}, μ_a≈0.2 mm^{-1}.

sured and simulated data indicates that the results from the expanded Monte Carlo simulations (model 2) reflect measurements with ideal geometry.

4.2 Influence of the Optical Properties

The influence of optical properties on LDF perfusion was studied in a more general way by evaluating ΔPerf [Eq. (7)], using perfusion data from the expanded simulations (model 2). Figures 6(a)–6(d) indicate that an increase in either the scattering or the absorption coefficient will result in a decrease of LDF perfusion. Specifically, the findings show that the influence of the change in absorption coefficient on the LDF perfusion is rather weak for the most superficial disks, but increases rapidly for larger disk depths [Figure 6(a) vs 6(b)]. According to Figures 6(c) and 6(d), the influence of change in the scattering coefficient on LDF perfusion increases almost linearly with an increase in disk depth. Figures 6(a)–6(d) also indicate that the simulated LDF perfusion readings seem to be affected slightly more by changes in the scattering coefficient than to changes in the absorption coefficient, at least for the most superficial disks. It is also clear that the influence of optical properties on LDF perfusion is not only affected by the change in scattering or absorption coefficient, but also by the magnitude of the nonchanged coefficient. For example, a change in the absorption coefficient has a larger impact on LDF perfusion when the scattering coefficient is relatively large [Figure 6(a) vs 6(b)]. This can be understood by realizing that a larger scattering level will increase the path length of the photons detected, thus making the effect of absorption and changes in absorption larger. The same is valid for a change in the scattering coefficient [Figure 6(c) vs 6(d)]. These results show that it is not only the optical properties or the actual flow depth that affects the LDF perfusion, but rather a combination of both. One way of interpreting this result is that the optical properties affect the sampling depth and thereby make the LDF readings sensitive to the actual flow depth.

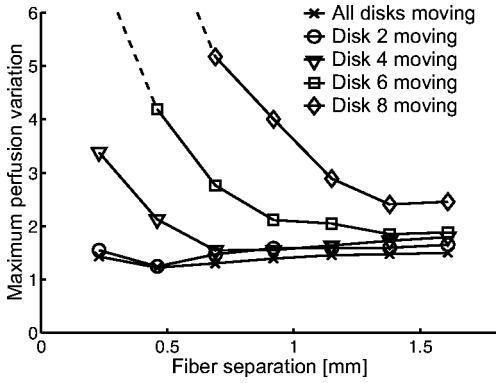

Fig. 7 Simulated maximum perfusion variation, due to variations in the optical properties, for a homogeneous distributed flow model (model 2 with all disks moving) and a discrete flow model (model 2 with single disks moving).

By increasing the fiber separation the influence of optical properties on LDF perfusion decreased when measuring at discrete disk depths. This effect is most pronounced when a change in the scattering coefficient occurs [Figure 6(c) vs

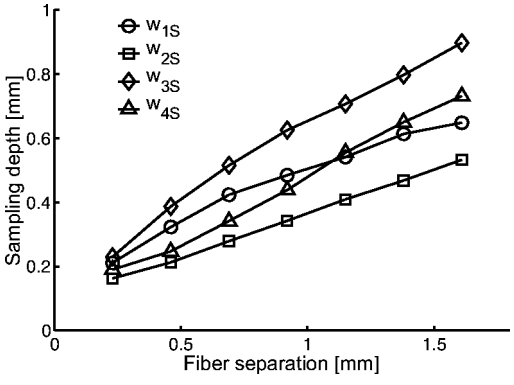

Fig. 8 Simulated (model 2) e^{-1} LDF sampling depth for a range of fiber separations (0.23–1.61 mm) and optical properties (w_{1s}–w_{4s}).

6(d)]. However, all perfusion readings on human skin originate from photons that have been Doppler shifted at different skin depths. This means that the depth distribution of the scattering events of the detected photons, i.e., the sampling depth, will affect the perfusion measured. This distribution is not only determined by the optical properties of the sampling volume but also by the fiber separation; an increase in fiber separation will increase the sampling depth. As mentioned before, the influence of optical properties on LDF perfusion is greater for deep blood flow than for superficial. Therefore, an increase in fiber separation does not guarantee that the influence of optical properties on LDF perfusion decreases when measuring distributed blood flow (e.g., human skin). This is illustrated in Figure 7, where a both homogeneous and discrete flow distribution model is assumed. In the case in which all disks move, the maximum perfusion variation [Eq. (7)] is somewhat independent of the fiber separation, on average 40% and ranging from 22% to 50%. Figure 7 also indicates that the maximum perfusion variation increases with the flow depth. Therefore, it is logical to assume that the maximum perfusion variation is even greater when studying real tissue, where the unknown heterogeneous blood perfusion distribution is assumed to increase with the skin depth.

4.3 Sampling Depth

Assume a homogeneous blood flow distribution, no multiple Doppler shifts and that the distribution of the photons scattering events detected decreases exponentially with the depth. The definition of sampling depth used then implies that ~63% of the perfusion signal is generated in the region above this depth. According to Figure 8 the LDF sampling depth increases with an increase in fiber separation. It is also obvious that the optical properties have a strong influence; an increase in either scattering or the absorption coefficient will result in a decrease in sampling depth. Similar trends of the absorption coefficient for fiber separations larger than 1 mm have previously been reported by Weiss et al.[6] However, their predictions of the sampling depth were larger than ours, probably because they used a lattice random-walk model with a point source and a point detector. The influence of probe geometry, using Monte Carlo simulations, has previously been investigated by Jakobsson et al.[5] They found similar trends with regard to fiber separation but a more superficial sampling depth than we found, probably because they studied the median depth of the photons pathways detected.

5 Conclusions

There was good agreement between measured and simulated data, indicating that the results from the expanded Monte Carlo simulations (model 2) reflect measurements with ideal geometry. The simulations showed that an increase in either the scattering or the absorption coefficient of static tissue resulted in a decrease in LDF perfusion and the LDF sampling depth. Further, the simulations of a single rotating disk at discrete disk depth showed that the influence of the scattering coefficient and the absorption coefficient on LDF perfusion increased with an increase in disk depth. By increasing the fiber separation the influence of the optical properties on LDF perfusion decreased when simulating a single rotating disk. However, the sampling depth increased with fiber separation.

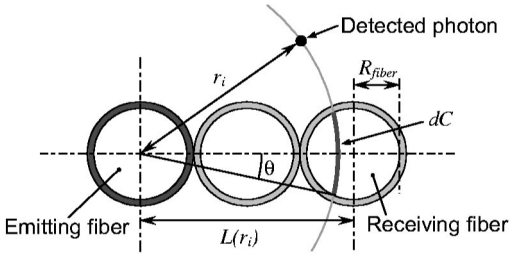

Fig. 9 Photon weights, when converting a ring shaped detector to a fiber detector (see the Appendix), can be calculated if the detection radius r_i, fiber separation $L(r_i)$ and fiber radius R_{fiber} are known.

This means that, for a distributed flow model, large fiber separation will result in a larger influence by the deepest lying flows that generate LDF perfusion values that are more sensitive to the optical properties, compared to a small fiber separation. Therefore, a increase in fiber separation will not guarantee a decrease in influence by the optical properties on LDF perfusion when measuring at a distributed blood flow. For a homogeneous flow distribution model, the maximum perfusion variation due to different optical properties was on average 40%, almost independent of the fiber separation.

Acknowledgments

This research was supported by the European Commission through Contract No. SMT4-CT97-2148. Under this contract, there is cooperation among Twente and Groningen (The Netherlands), Linköping and Malmö (Sweden), and Toulouse (France) Universities, and among Perimed AB (Sweden), Moor Instruments and Oxford Optronix (UK), and the Institute of Biocybernetics and Biomedical Engineering, Warsaw (Poland).

Appendix: Conversion of the Ring to Fiber Detector

In contrast to the measurements on the tissue phantom, a ring shaped detector (NA=1) was used to speed up the simulations. Therefore, to be able to compare the *in vitro* measurements with the simulations, all simulated photons had to be weighted differently depending on where they were detected. A photon, detected at distance r_i from the center of the emitting fiber (Figure 9), was weighted by p_i, defined as

$$p_i = \frac{dC}{2\pi r_i}, \tag{A1}$$

where dC is the fractional circumference given by r_i and limited by the border of the detecting fiber,

$$dC = 2r_i\theta. \tag{A2}$$

The law of cosines gives

$$R_{\text{fiber}}^2 = L(r_i)^2 + r_i^2 - 2L(r_i)r_i\cos(\theta). \tag{A3}$$

Combining Eqs. (A1)–(A3) results in

$$p_i = \frac{1}{\pi}\cos^{-1}\left(\frac{r_i^2 + L(r_i)^2 - R_{\text{fiber}}^2}{2 \cdot r_i L(r_i)}\right). \quad \text{(A4)}$$

This weight factor is only defined when the detection radius falls inside the core of one of the receiving fibers [$r_i \in (n0.23-0.1,\ n0.23+0.1);\ n=1,2,3,\ldots,7$]. Photons falling outside this range were assigned a weight factor of zero. The distance between emitting and receiving fibers (L) depends on the simulated detection radius (r_i) and is given by

$$L(r_i) = n0.230 \text{ mm}, \quad n = \text{round}\left(\frac{r_i}{0.23}\right). \quad \text{(A5)}$$

References

1. R. F. Bonner and R. Nossal, ''Principles of laser-Doppler flowmetry,'' in *Laser-Doppler Blood Flowmetry*, A. P. Shepherd and P. Å. Öberg, Eds., pp. 17–45, Kluwer Academic, Norwell, MA (1990).
2. A. Liebert, M. Leahy, and R. Maniewski, ''Multichannel laser-Doppler probe for blood perfusion measurements with depth discrimination,'' *Med. Biol. Eng. Comput.* **36**(6), 740–747 (1998).
3. K. Johansson, A. Jakobsson, K. Lindahl, J. Lindhagen, O. Lundgren, and G. E. Nilsson, ''Influence of fibre diameter and probe geometry on the measuring depth of laser Doppler flowmetry in the gastrointestinal application,'' *Int. J. Microcirc.: Clin. Exp.* **10**(3), 219–229 (1991).
4. H. W. Jentink, F. F. M. de Mul, R. G. A. M. Hermsen, R. Graaff, and J. Greve, ''Monte Carlo simulations of laser Doppler blood flow measurements in tissue,'' *Appl. Opt.* **29**(16), 2371–2381 (1990).
5. A. Jakobsson and G. E. Nilsson, ''Prediction of sampling depth and photon pathlength in laser Doppler flowmetry,'' *Med. Biol. Eng. Comput.* **31**(3), 301–307 (1993).
6. G. H. Weiss, R. Nossal, and R. F. Bonner, ''Statistics of penetration depth of photons re-emitted from irradiated tissue,'' *J. Mod. Opt.* **36**(3), 349–359 (1989).
7. T. Tenland, E. G. Salerud, G. E. Nilsson, and P. A. Oberg, ''Spatial and temporal variations in human skin blood flow,'' *Int. J. Microcirc.: Clin. Exp.* **2**(2), 81–90 (1983).
8. G. E. Nilsson, T. Tenland, and P. Å. Öberg, ''A new instrument for continuous measurement of tissue blood flow by light beating spectroscopy,'' *IEEE Trans. Biomed. Eng.* **27**(1), 12–19 (1980).
9. R. A. Bolt, J. S. Kanger, and F. F. M. de Mul, ''Angular dependence of light scattering by biological tissue,'' *Proc. SPIE* **3570**, 168–173 (1998).
10. W. Steenbergen and F. F. M. de Mul, ''Description of an improved laser Doppler calibrator,'' *Proc. SPIE* **3599**, 68–75 (1999).
11. W. Steenbergen and F. F. de Mul, ''New optical tissue phantom, and its use for studying laser Doppler blood flowmetry,'' *Proc. SPIE* **3196**, 12–23 (1997).
12. W. Steenbergen and F. F. de Mul, ''Application of a novel laser Doppler tester including a sustainable tissue phantom,'' *Proc. SPIE* **3252**, 14–25 (1998).
13. G. E. Nilsson, A. Jakobsson, and K. Wårdell, ''Tissue perfusion monitoring and imaging by coherent light scattering,'' *Proc. SPIE* **1524**, 90–109 (1991).
14. G. E. Nilsson, T. Tenland, and P. A. Oberg, ''Evaluation of a laser Doppler flowmeter for measurement of tissue blood flow,'' *IEEE Trans. Biomed. Eng.* **27**(10), 597–604 (1980).
15. S. T. Flock, M. S. Patterson, B. C. Wilson, and D. R. Wyman, ''Monte Carlo modeling of light propagation in highly scattering tissue I: Model predictions and comparison with diffusion theory,'' *IEEE Trans. Biomed. Eng.* **36**(12), 1162–1168 (1989).
16. S. T. Flock, B. C. Wilson, and M. S. Patterson, ''Monte Carlo modeling of light propagation in highly scattering tissues. II: Comparison with measurements in phantoms,'' *IEEE Trans. Biomed. Eng.* **36**(12), 1169–1173 (1989).
17. L. G. Henyey and J. I. Greenstein, ''Diffuse radiation in the galaxy,'' *Astrophys. J.* **93**, 70–83 (1941).
18. F. F. M. de Mul, M. H. Koelink, and M. L. Kok, ''Laser-Doppler velocimetry and Monte-Carlo simulations on models for blood perfusion in tissue,'' *Appl. Opt.* **34**(28), 6595–6611 (1995).